ISSN 0016-8521, Geotectonics, 2013, Vol. 47, No. 6, pp. 418–430. © Pleiades Publishing, Inc., 2013.
Original Russian Text © V.G. Trifonov, 2013, published in Geotektonika, 2013, Vol. 47, No. 6, pp. 3–17.

Cyclicity of Late Holocene Seismicity in the Alpine–Himalayan Belt

V. G. Trifonov

Geological Institute, Russian Academy of Sciences, Pyzhevskii per. 7, Moscow, 119017 Russia
e-mail: trifonov@ginras.ru

Received January 20, 2013

Abstract—It has been shown for particular seismic zones and the Alpine–Himalayan Orogenic Belt as a whole that in addition to Fedotov cycles, the long-period hypercycles of seismicity are distinguished. Long-period variations were revealed in Syria, in southern and central segments of the El-Ghab Fault Zone of the Dead Sea Transform (EG DST), and at the southwestern end of the East Anatolian Fault Zone (EAFZ). The EG DST demonstrates a ~1800-year hypercycle with a maximum in the 3rd–7th and the 19th–20th centuries A.D. To reveal variations in seismicity in the entire central part of the orogenic belt, we have corrected evidence for historical earthquakes, taking into account the probability of missing events and the area of their regular recording domains. As a result, we displayed maximums of seismic energy release from the mid-17th to mid-20th century A.D.; from the mid-4th to the end of the 6th century; and in the 15th–13th centuries B.C. When interpreting hypercycles, it is important to keep in mind that variation of seismicity in EG DST correlates with variation of the rate of elastic deformation accumulation, probably reflecting variability of the stress-and-strain state in the region and of velocity of tectonic movements in active domains. After additional investigations, hypercycles could be taken into account for to refine the seismic hazard estimate.

DOI: 10.1134/S001685211306006X

INTRODUCTION

The averaged characteristics of natural processes are commonly used in geological practice, for example, the average rate of sedimentation or velocity of tectonic movements (subsidence or uplifting of structural elements). Such averaging is induced by lack or inaccuracy of knowledge primarily on the age of geological objects and events. This is also valid for the recent stage of the Earth's evolution. In spite of more fractional chronostratigraphic subdivision and correlation of objects, data on the Pliocene–Quaternary epoch as usual have remained averaged.

When dealing with the contemporary epoch, it becomes evident that many geological events have occurred extremely nonuniformly in time and that their products are series of discrete manifestations. Examples are the products of downfalls, landslides, mudflows, volcanic eruptions, and offsets during strong earthquakes. At the same time, the period of observations for which precision instrumental rate determination methods are available (precision dating of events; estimation of composition, thickness, and volume of sediments; parameters of earthquakes; and contemporary movements of the Earth's surface deduced from data of recurrent geodetic observations) is commonly limited to the last century. The interval of such observations can be widened on the basis of reliable historical records, archeological and radioisotopic, e.g., radiocarbon methods, the accuracy of which for the last centuries attains tens of years when the quality of analyzed material is good. The rate determination accuracy in these cases occasionally decreases by orders of magnitude, and the risk of mistake (omission of target) appears. In any case, the period of contemporary observations, even when increased by historical digressions, is too small to deem it representative for estimating the regime of geological processes.

To comprehend the relationships between geological manifestations on an everyday time scale, when individual events are recorded, and on a geological time scale based on averaged effects of events, we have to rely on a time interval that allows us to study natural phenomena on both everyday and geological time scales. Hundreds and a few thousands of years are suitable for many geological phenomena in this respect.

Long-term series of strong recorded earthquakes have been chosen in this study as the most universal indicators of geodynamics in tectonically active domains. The central segment of the Alpine–Himalayan Orogenic Belt and especially the eastern Mediterranean region offers a unique opportunity, owing to three circumstances [4, 6]. First, the regular recording of earthquakes started here approximately from somewhere in the 1st millennium B.C. Second, many archeological memorials with indications of seismic impacts have been retained. Third, some strong earthquakes have been revealed and parameterized as a result of paleoseismological investigations. The joint use of these sources of information made it possible to create catalogs of earthquakes in the seismotectonic zones and provinces of this belt, where regular (no less than two events per century) recording of seismic

events has been carried out during the last 2500–5000 years, i.e., over the time interval considered by us. Note that if a record of strong historical earthquake is based on information on damage in a single settlement and not supported by archeo- or paleoseismological evidence, the compilers of catalogs had to ascribe this event to this locality. In the seismotectonic interpretation of such earthquakes near the town of Aleppo in Syria, we followed the route proposed in [20] and referred them to the nearest fault in the seismoactive northern segment of the El-Ghab Fault Zone at a distance of 10–15 km from Aleppo.

The main parameter used to estimate time-dependent variations in seismicity of the considered territories was the amount of energy released during earthquakes. This parameter was calculated in joules using the equation proposed by F.T. Aptikaev [4] and related energy E to magnitude M_S:

$$E = 10^{(8.1+0.9098(M+1.55))}.$$

Earthquakes in the Alpine–Himalayan Belt considered below are crustal and, as a rule, related to large active fault zones and attendant disturbances. An earthquake is defined as a result of offset along a fault or several faults. An individual offset can be calculated from the seismic parameters of the earthquake. Displacements and deformations of the Earth's surface and near-surface ground in the fault zone during strong earthquakes are revealed using geological and geomorphic methods. The average velocities of movements along the fault are estimated from offsets of dated geological bodies over the Holocene or late Holocene, i.e., over a time interval close in duration to that considered in this paper. In some cases, the established offset or its vertical component may be interpreted as the cumulative effect of several revealed earthquakes. All this allows us to compare individual events and their averaged characteristics, i.e., to lay a bridge between everyday and geological time.

Based on an analysis of time-dependent series of seismicity, Fedotov [9] introduced the notion of a seismic cycle characterizing variations in the number and intensity of earthquakes in an active zone with a more or less persistent period of recurrence. Such cycles are recognized in many but not in all active zones and are commonly interpreted as a periodic release of accumulated elastic deformation. It is assumed that the rate of such accumulation is constant. The aim of this paper is to show that in addition to these cycles, longer variations of seismicity (hypercycles), which are probably related to the stress-and-strain state of active zones and their strength, are outlined. These hypercycles are exemplified below in separate active zones and the central Alpine–Himalayan Belt as a whole.

NORTHERN SEGMENT OF THE DEAD SEA TRANSFORM

The Dead Sea Transform (DST) is the western boundary of the Arabian lithospheric plate and consists of several branches [4, 8, 18, 37, 45]. These are the major DST segments arising in the Pliocene: Yamounneh in Lebanon and El-Ghab in southern Turkey; the Rashaya, Serhaya, St. Simeon, and smaller splays; and the Roum Fault inherited from the Miocene DST structure and the Tartous Fault Zone continuing it on the continental slope of the Mediterranean Sea (Fig. 1). The aforementioned faults reveal attributes of late Quaternary left-lateral strike-slip offsets with a subordinate vertical component. The inherited faults are characterized by relatively low contemporary activity. The El-Ghab Fault Zone is conjugated in the north with the southwestern end of the active East Anatolian Fault Zone (EAFZ), which is characterized by a left-lateral reverse–strike-slip offset and passes in the west into the active southern framework of the Cyprus arc with signs of slow subduction.

The objects under consideration are earthquakes in the El-Ghab Fault Zone consisting of southern, central, and northern subsegments differing in structure [4, 8, 37]. Historical earthquakes with $M_S \geq 5.7$ and earthquakes of the 20th century A.D. with $M_S \geq 5.0$ are considered (Table 1). Because of inaccurate tying of historical earthquake hypocenters, it is impossible to attribute the earthquakes at the El-Ghab–EAFZ junction to one of these zones with confidence. Therefore we so far omit the northern subsegment from consideration and confine ourselves to the central and southern subsegments between 34.5° and 36.15° N, where 30 historical earthquakes with $M_S \geq 5.7$ and none earthquakes with $M_S \geq 5.0$ in the 20th century A.D. have been recorded.

When analyzing the time-dependent distribution of amounts of seismic energy released by earthquakes, we find that strong earthquakes repeated with a periodicity of 350 ± 50 Ma (Table 2; Fig. 2a). This recurrence, supported by archeo- and paleoseismological evidence in the southern subsegment of the El-Ghab Fault Zone [31], can be regarded as a manifestation of seismic cycles. Nevertheless, it turns out that the amount of energy released during the maximum phase of a seismic cycle varies from one to another. The moderate amount of energy in the 1st century A.D. decreased in the 5th century and then increased to a maximum in the 12th century. The amount of energy decreased, remaining rather high during the maximum phase of the next cycle (15th century) and then abruptly fell to a complete absence of earthquakes with $M_S \geq 5.0$ in the 20th century. Thus, a hypercycle with a period of ~1800 yr is superposed on the cyclicity with a period of 350 ± 50 Ma.

Several strong seismic events occurred in the 12th century in the south and center of the El-Ghab Fault Zone. The strongest was the June 29, 1170,

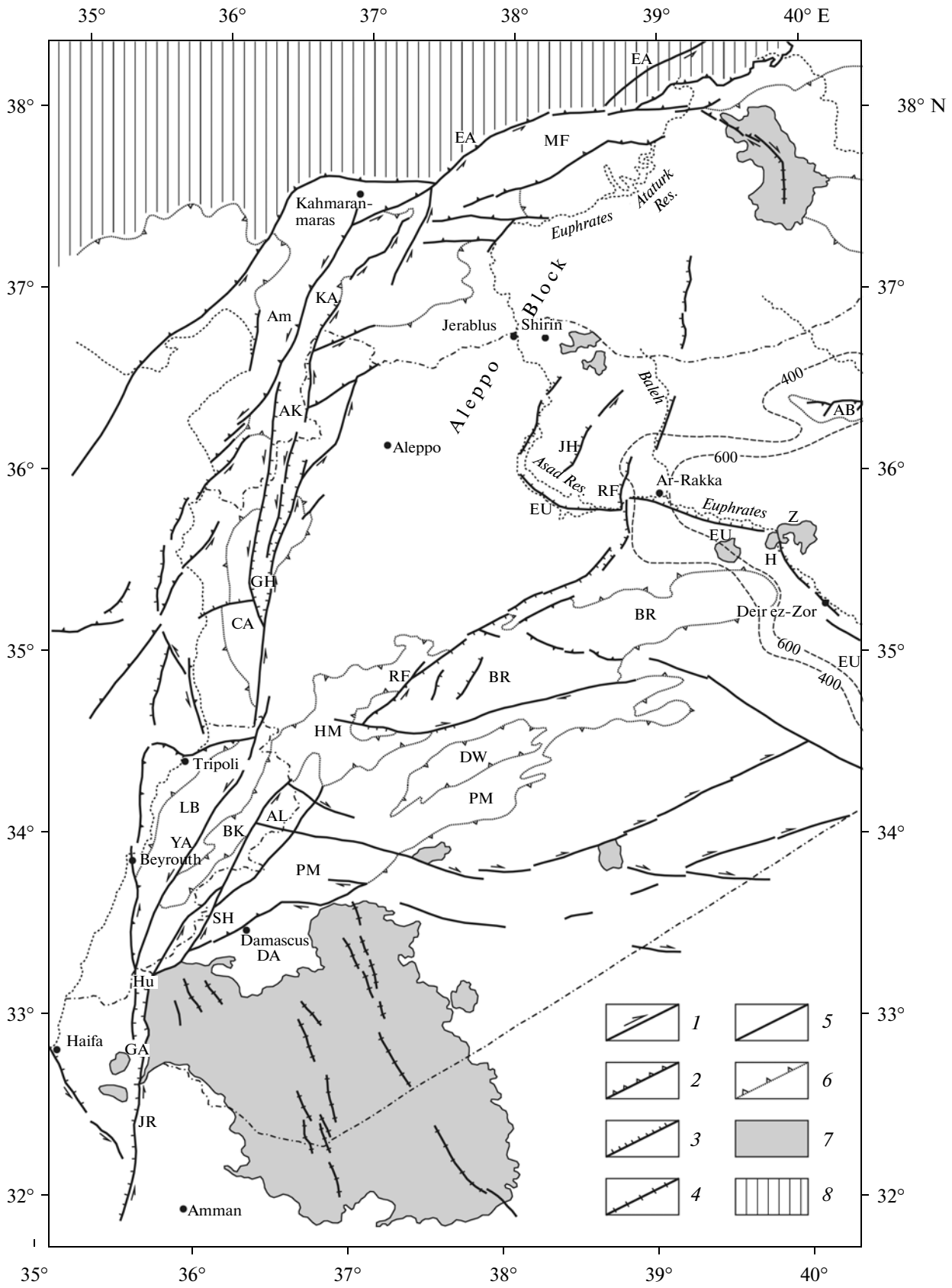
35°
36°
37°
38°
39°
40° E
38° N
37°
36°
35°
34°
33°
32°
EA
MF
Kahmaran-
maras
Euphrates
Atatürk
Res.
KA
Am
Jerablus
Shirin
Block
Aleppo
Aleppo
Balen
400
AB
AK
JH
600
Asad Res.
RF
Ar-Rakka
EU
Euphrates
Z
EU
H
GH
CA
BR
Deir ez-Zor
600
EU
400
RF
BR
HM
DW
PM
Tripoli
LB
AL
BK
YA
Beyrouth
PM
SH
Damascus
DA
Hu
Haifa
GA
JR
Amman
1
2
3
4
5
6
7
8

Fig. 1. Late Pliocene–Quaternary (last 3.5 Ma) structural elements of northern Arabian Plate. Miocene isopachs of 400 and 600 m display structure of Mesopotamian Trough. (*1*) Strike-slip fault; (*2*) reverse and thrust faults; (*3*) normal fault; (*4*) pull-apart fault; (*5*) fault with unspecified type of displacement; (*6*) boundaries of uplifts and basins; (*7*) Late Cenozoic basalts; (*8*) Alpine–Himalayan Belt. *Anticlines and zones of uplifts:* AB, Abdelaziz; AL, Antilivan; BR, Bishri, Northern Palmirides; CA, Coastal Range of Syria; LB, Lebanon Range; MF, belt of marginal folds of Turkey; PM, Southern Palmirides; *faults and fault zones:* Am, Amanos, EAFZ segment; EA, East Anatolian Fault Zone; EU, Euphrates; JH, Bir Jabel–Haymar al Kabir; JR, Jordan segment of DST; RF, Rasafe-Faid; SH, Serhaya; YA, Yamounne segment of DST; *basins:* AK, Amik; BK, Bekaa Syncline; DA, Damascus; DW, Ad-Dau; GA, pull-apart basin of Sea of Galilee, DST; GH, El-Ghab pull-apart basin, DST; HM, Homs Basin; Hu, Hula pull-apart basin, DST; KA, Karasu Graben.

earthquake with $M_S = 7.7$. According to macroseismic data [19, 35, 38, 41], an area of quakes with an MSK intensity number of VIII is traced along the El-Ghab Fault Zone from Joubeil and Baalbak to Shayzar and Aleppo (Fig. 3). Tripoli was completely destroyed, and the intensity there could have reached an MSK number of IX. This gave grounds to place epicenter at the junction of the El-Ghab and Yamounneh fault zones [38]. Other authors, using data on significant destruction in Aleppo and Lattakia, placed the epicenter in the pull-apart basin of the central subsegment of the El-Ghab Fault Zone [14, 19].

Information on the settlements damaged in 1170 does not involve the territory immediately adjoining the El-Ghab Fault Zone. Let us consider evidence for this zone in detail. The Crack de Chevalier Fortress is situated at its southern end. Since the 11th century A.D. it was the property of the Hospitalier Order until was occupied by Mameluks in 1271. If insignificant late rebuilding is ruled out, the erection of the main constructions still standing today was completed by 1207. As shown by an archeological study in its southern part, they were built at the place of previously destroyed structures. For example, one of southern round towers had been erected at the place of a destroyed tower, the retained basement of which has rectangular outlines. The southern aqueduct that provided the fortress with water bore attributes of twofold destruction and rebuilding. When did this destruction happen? Historical sources inform that the fortress was affected by earthquakes in 1157, 1170, and 1202. Damage in 1157 was insignificant, because immediately afterward the fortress retained its defensive function. The rebuilding of the fortress was finished in 1188–1189, when it withstood an attack by Saladin's army. Afterward, the fortress was attacked repeatedly but remained an advanced post for crusaders up to 1271 despite an earthquake in 1202. Thus, the main destruction was related to the 1170 earthquake and indicate that its intensity had an MSK number of ~XI.

The second object crucial for estimating the intensity of quakes in 1170 was the Roman aqueduct in the southern subsegment of the El-Ghab Fault Zone near Al-Harif (Fig. 3). According to archeological evidence, the aqueduct was built in the 1st century B.C. to the 1st century A.D., no earlier than 63 B.C., and then displaced ~12 m along the fault [4, 31, 37, 39]. Trenching of the fault zone showed that this offset was the cumulative effect of at least three strong earthquakes; 1170 was the latest [31]. At that time, the offset could have reached 4 m and the intensity of quakes near the aqueduct had an MSK number of IX and X.

Thus, the domain of 1170 quakes with an MSK number of XI can be presumably outlined along the southern subsegment of the El-Ghab Fault Zone, and the epicenter can be placed within this zone. Judging by the extent of the domain of MSK numbers of VIII to IX and inferred seismogenic offset, the earthquake's magnitude reached $M_S = 7.7$. These parameters of the 1170 earthquake are presented in Table 1. The 1170 seismic event is comparable in size of the epicentral domain and magnitude to the earthquake of May 20, 1201 ($M_S = 7.6$). Its epicenter is confined to the Yamounneh DST; however, the isoseist of MSK number VIII contouring it also spreads over a significant part of the Jordan segment of the DST [15] (Fig. 3).

From the tectonophysical viewpoint, any earthquake implies that acting stresses exceed the ultimate strength due to increasing stress or decreasing strength. The force (magnitude) of an earthquake depends on the volume of rock where the ultimate strength is achieved and the stored stresses (elastic deformation) relax. In the given case, this is the volume of the El-Ghab Fault Zone. Because all earthquakes occurred at similar depths in the Earth's crust, the volume was determined by the total length of the activated part of the DST, which became equal to the total length of the El-Ghab segment (~230 km) at the peak rate of accumulation of elastic deformation (1170 earthquake, MWS = 7.7) and it was smaller during other earthquakes.

Two alternative interpretations have been proposed for the decline of seismicity after the first decade of the 15th century A.D. and the contemporary seismic quiescence in the south and center of the El-Ghab Zone. According to the first explanation, the decline and quiescence are precursors of a forthcoming superstrong earthquake in the near future [31]. The second explanation assumes that the decline and quiescence reflect a decrease in the level of seismic activity in this zone [4]. In accordance with the hypercycle tendency, the magnitude of the strong earthquake expected in the future will most likely be no higher than magnitudes of the cycle at threshold of the 19th century A.D. ($M_S = 6.5–7.0$); in any case, it will not reach the $M_S = 7.7$ magnitude of the 1170 earthquake. The second scenario becomes more plausible if it is assumed that the amount of released energy varies in proportion to

Table 1. Catalog of strong and perceptible earthquakes in El-Ghab Fault Zone and southwestern East Anatolian Fault Zone, Syria and adjacent territories

A. Catalog of historical earthquakes with magnitudes $M_S \geq 5.7$

No.	Year	Month	Day	Zone	Reference	φ	λ	M_S	I_0	H
1.	37	–	–	1	40	36.0	36.3	6.2	7–8	15
2.	47–48	–	–	1	17	35.7	36.30	6.7	7	20
3.	53	–	–	1	36, 38	36.2	36.5	7.0	8	30
4.	75			4	22	38.8	41.3	6.5	10	
5.	76–82–94	–	–	2, 4	30, 34, 40	36.25	36.10	6.5	7	16
6.	97	–	–	4	26	37.3	36.3	6.2	9	
7.	128–130	–	–	2, 4	29, 34, 40	37.30	36.80	6.0	6–7	
8.	220	–	–	2, 4	29, 38	36.30	36.10	6.1	–	–
9.	245	–	–	4	34, 38, 40	37.30	36.50	7.6	10	–
10.	272	–	–	2, 4	29, 34, 38	36.25	36.10	6.1	>6	
11.	290	5	14	2, 4	29	36.25	36.10	6.1	–	–
12.	293	3	06	4	17	37.06	35.80	7.4	–	–
13.	334			2, 4	30, 34, 40	36.5	36.1	6.8	9	
14.	344–345	–	–	2, 4	34, 40	36.25	36.10	5.7	5–6	
15.	348–349	–	–	2, 4	17, 26, 30, 34	36.25	36.10	7.0	8–10	23
16.	394–396	–	–	2	30, 36, 38, 40	36.3	36.3	6.5	7–8	
17.	419	–	–	2, 4	17, 26, 34	36.25	36.10	6.1	7–8	–
18.	458	9	14	1	17, 29, 34, 38	36.2	36.4	7.7	9	20
19.	477			1	40	35.3	35.9	5.7		
20.	494	–	–	1	34, 38	35.80	36.30	6.6	8	25
21.	499–500	–	–	4	14, 22, 26, 30, 34, 40	38.13	38.63	7.5	8–10	–
22.	517–518	–	–	4	29, 40	37.20	35.90	6.1	–	–
23.	518	5	–	2, 4	29, 40	36.25	36.10	6.1	–	–
24.	521	–	–	2, 4	30	36.88	36.60	7.4	–	40
25.	524	–	–	4	29, 40	37.30	36.30	6.1	–	–
26.	526	5	20/29	2, 4	19, 27, 34,38, 43	36.2	36.1	7.5	10	–
27.	528	11	29	2	27, 34, 38	36.25	36.83	7.5	10–11	–
28.	553			2, 4	38, 40	36.3	36.1	5.7		
29.	557	10	19	1	29, 38	36.1	35.55	6.0	–	–
30.	565–571	–	–	1	29, 38	36.0	36.20	6.0	7–8	30
31.	580–581	–	–	2	26, 34, 40	36.25	36.30	5.7	–	–
32.	587–588	9/10	30/31	4	26, 34, 40	37.50	36.00	6.9	9	–
33.	634			3	30, 35, 36	36.23	37.17	6.3	8	
34.	639			2	38, 40	36.3	36.1	5.7		
35.	678			4	26	38.20	39.50	7.7	10	26
36.	713	2	28	1	26, 30, 35, 36, 38	35.70	36.30	7.0	9	–
37.	717	12	24	2, 4	29, 38, 40	36.25	36.10	6.1	–	–
38.	757	3	09	4	35, 36, 38	37.00	35.60	5.7	7	
39.	775	–	–	4	29, 38	36.95	35.58	6.7	–	
40.	791			2	30, 38, 40	36.2	36.7	6.8		30
41.	803	–	–	4	34, 35, 36	37.0	35.6	6.0	8	
42.	835			4	26, 30, 35, 36, 38, 40	36.8	36.3	6.1	>7	
43.	860	1		1	17, 29, 38	35.70	36.40	7.4	9–10	33
44.	867			3	34, 40	36.25	36.10	6.5	9	
45.	951	9		3	34, 38, 43	36.20	37.20	6.8	8–9	–
46.	963	7	22	2	29, 38, 40	36.60	37.0	6.1	–	–
47.	972	10	12	2	26, 29, 40	36.60	37.00	6.9	9	–
48.	995	12	31	4	14, 22, 30, 40	38.7	40	7.5		
49.	1002–1003	–	–	2	30, 38	36.50	36.50	6.8	>8	–
50.	1091	9/10	26/06	1	29, 38	36.35	36.10	7.4	9	–
51.	1094	4–5	–	1	34, 38, 43	35.90	36.30	6.0	6	–

Table 1. (Contd.)

No.	Year	Month	Day	Zone	Reference	φ	λ	M_S	I_0	H
52.	1114	11		4	38	37.30	36.50	7.7	9	40
53.	1138	10	11/26	3	33–36, 38, 40	36.3	37.2	6.8	10	
54.	1140–1141			3	29, 38	36.23	37.17	6.1	7	–
55.	1157	4	02/04	1	38	35.50	36.50	6.0	7	22
56.	1157	7	13	1	19, 35, 38	35.20	36.60	6.6	8	25
57.	1157	8	12	1	12, 14, 35, 38	35.40	36.50	7.4	9–10	15
58.	1170	6	29	1	14, 26, 31, 34–36, 38	35.0	36.30	7.7	9–10	35
59.	1183–1190	9	–	1	29	36.00	36.30	6.1	–	–
60.	1212			2, 4	29, 38	36.20	36.10	6.1		
61.	1222			3	29, 38	36.3	37.1	5.9		
62.	1290–1292			1	34, 38	35.15	36.73	6.8	8	–
63.	1403	12	18	3	38	36.20	37.10	5.7	–	–
64.	1404	2	20	1	35, 36, 38	35.70	36.20	7.4	9	30
65.	1404	11–12		1	35, 36, 38	35.70	36.20	5.7	6	
66.	1407	4–5	–	1	12, 14, 16, 29, 35, 38	35.7	36.4	7.0	10	–
67.	1408	12	29	1	16, 35, 36, 38	35.80	36.10	7.4	9–10	25
68.	1484	3/4	29/27	2	35, 36, 38	36.20	36.75	6.4	7	–
69.	1513			4	22, 30, 34	37.5	36.5	7.4		
70.	1537	1	07	1	29, 30, 38	35.8	36.3	6.4		20
71.	1568	10	10	4	38	35.50	35.50	6.0	8	12
72.	1577	1	28	1	30, 35, 38	35.50	36.50	6.6	–	–
73.	1610	3	7	2	13, 38	36.2	36.8	5.7	>6	
74.	1626	1	21	2	13, 38	36.50	37.10	7.3	9	20
75.	1656	2		1	19, 35, 38, 40	34.60	36.40	6.6	8–10	–
76.	1691			4	22	38.6	40	6.0	8	
77.	1719	3		2	29, 35, 40	36.50	36.9	6.4	>7	20
78.	1726	4	15	2	29, 38, 40	36.30	36.60	6.1	8	15
79.	1738	9	25	2, 4	38	36.70	36.50	6.2	8	10
80.	1752	7	21	4	38, 40	35.20	35.30	6.8	>7	–
81.	1759	1	12	4	22	38.3	38.3	6.5	9	
82.	1759	2	17	3	34, 38, 43	36.20	37.10	6.6	8	–
83.	1760	1		2	34, 35	36.2	36.8	6.4	8	–
84.	1765			1	13, 35, 40	34.50	36.35	6.4	–	–
85.	1779	6	08	3	13, 29	36.20	37.10	5.7	–	–
86.	1783	7	20	1	30, 35, 40	35.6	36.40	6.5	–	–
87.	1789	5	29	4	14, 22, 30, 34	39.0	40.0	7.0	8	
88.	1796	4	26	1	12, 13, 34, 35, 38	35.30	36.30	6.8	8–9	20
89.	1822	8	13	1	11, 19, 35, 36, 38, 42	36.10	36.75	7.0	9	18
90.	1822	9	05	1	36, 38	36.10	36.75	5.7	7	
91.	1831	2	22	3	29, 38, 40	36.20	37.10	5.7	>5	–
92.	1845–1847			4	38, 40	36.60	36.10	5.7	–	–
93.	1859	1	24	4	35, 38	34.70	35.25	5.7	–	–
94.	1866	7	20	4	3, 40, 42	38.4	39.4	6.1	8	15
95.	1872	4	03	2	11, 12, 19, 29, 36, 38	36.2	36.50	7.2	9–10	10
96.	1872	5	15	2, 4	40	36.2	36.1	5.7		
97.	1874	5	03	4	14, 22, 30, 40, 42	38.5	39.5	7.1		14
98.	1875	3	03/27	4	3, 19, 22, 40, 42	38.5	39.5	6.7	9	
99.	1884	6	06	3	38	36.30	37.20	5.7	>5	–
100.	1893	3	12/31	4	14, 22, 30, 33, 40, 42	38.10	38.40	7.1	9	21
101.	1894	5	14	4	30	36.60	35.60	6.1	–	30

Table 1. (Contd.)

B. Catalog of instrumental earthquakes with magnitudes

No.	Year	Month	Day	Hour:min	Zone	Reference	φ	λ	Mr	I_0	H
1.	1900	11	10	16:23	4	30	38.08	38.72	5.4		
2.	1905	12	04	07:04	4	14, 30	38.12	38.63	6.8	9	18
3.	1905	12	04	09:40	4	28, 30, 35	38.0	38.3	5.8		
4.	1908	2	17	03:00	4	28, 30, 34	37.4	35.8	6.0	8	33
5.	1908	09	28	06:28	4	3, 30	38.5	39.2	6.1	6	32
6.	1908	10	30	11:00	4	25, 30	37.6	36.8	5.4		
7.	1915	12	25	06:06	4	25, 30	36.47	36.14	5.4		10
8.	1921	10	05	19:09	4	25	36.4	35.2	5.5		33
9.	1931	05	06	20:22	4	25, 30	38.24	39.15	5.0		40
10.	1936	06	14	17:01	4	30	36.5	36.0	5.5		
11.	1948	08	18	19:06	4	25, 30	38.9	39.4	5.0		10
12.	1949	04	25	23:09	4	25, 30	38.27	38.99	5.3		80
13.	1950	11	08	10:07	4	25, 30	38.3	39.1	5.2		33
14.	1951	04	08	21:38	4	25, 28, 30, 34	36.58	35.85	5.8	8	
15.	1953	03	24	21:17	2	25, 30	37.02	37.0	5.2		10
16.	1961	06	01	16:31	4	25, 30	37.65	36.76	5.0		40
17.	1964	06	14	12:15	4	25, 30, 33, 34	38.10	38.50	6.0		10
18.	1967	04	07	18:33	4	33	37.345	36.175	5.0		33
19.	1971	05	22	16:43	4	14, 21, 22, 25, 30, 33	38.85	40.52	6.8	8–9	20
20.	1971	06	29	09:08	2	30, 33	37.12	36.84	5.3		35
21.	1971	07	11	20:12	2	21, 30, 33	37.17	36.8	5.6		16
22.	1971	08	17	04:29	2	33	37.099	36.819	5.0		33
23.	1979	09	12	16:14	4	33	38.662	39.803	5.0		10
24.	1981	01	20	08:27	4	33	38.079	38.473	5.1		10
25.	1986	05	05	03:35	4	25, 30, 33	38.00	37.80	5.9		8
26.	1986	06	06	10:39	4	25, 30, 33	38.01	37.91	5.7		10
27.	1986	08	03	01:33	2	33	37.20	37.30	5.0		12
28.	1991	04	10	01:08	4	33	37.359	36.221	5.2		10
29.	1992	05	07	19:15	4	33	38.698	40.143	5.0		18
30.	1994	01	03	21:00	4	33	37.002	35.842	5.0		26
31.	1997	01	22	17:57	4	33	36.25	35.951	5.7		10
32.	1997	01	22	18:24	4	33	36.239	35.922	5.2		10
33.	1997	01	22	18:27	4	33	36.275	35.997	5.3		10
34.	1998	05	09	15:38	4	33	38.278	38.988	5.1		10

φ and λ are latitude and longitude of the epicenter; Mr, type of magnitude indicated by source of information; I_0, intensity in epicenter; H, depth of hypocenter. Reference numbers correspond to the list of references. Zones: 1—southern and central El-Ghab, 2—northern El-Ghab, 3—Aleppo block, 4—SW EAFZ.

the rate of accumulation of elastic deformation within the fault zone. Let us consider to what extent this assumption is probable.

Over a long time, the accumulating elastic deformation was achieved in seismic offsets and residual deformations in the fault zone. The El-Ghab segment of thr DST arose in the Pliocene 4.0–3.5 Ma ago, and the average rate of the following Pliocene–Quaternary strike-slip faulting is estimated at 5 ± 1 mm/yr [4, 37]. This value has been determined in two ways. The elements of the late Miocene–early Pliocene structure on both sides of the fault were compared in [23, 24]. The offset is estimated at 16–20 km. By other means, the estimate is based on identification of ophiolitic

Table 2. Quantity of energy (10^{15} J) released by earthquakes in El-Ghab Fault Zone and southwestern East Anatolian Fault Zone (EAFZ) in Syria and adjacent territories

Century, A.D.	El-Ghab, south + center	El-Ghab, north	SW EAFZ	Century, A.D.	El-Ghab, south + center	El-Ghab, north	SW EAFZ
1	13	2.7	6.8	11	17.93	5	0
2	0	0.93	0.93	12	45.34	6.1	33
3	0	3.3	47.3	13	5	1.86	1.1
4	0	15.8	13.1	14	0	0	0
5	3.8	34.1	23.1	15	42.1	2.7	0
6	1.86	63.1	49.83	16	5.5	0	17.93
7	0	2.2	33	17	3.3	14.5	0.93
8	7.6	6.1	5.6	18	9.9	10.7	16.7
9	17	2.7	2.03	19	8.1	13.5	26.3
10	0	12.2	22	20	0	1.01	19.36

sections in the Bassit and Kurd Dagh districts and comparison of their southeastern boundary. To the west of the northern subsegment of the fault zone, the Lattakia Fault serves as this boundary; to the east, the boundary is the Aafrin Fault. Both faults strike to the northeast obliquely to the El-Ghab Fault Zone, which is ~20 km wide there. This introduces uncertainty into the estimate of the offset, which cannot be determined more accurately than 16–20 km [4]. Such an offset over the last 4.0–3.5 Ma gives an average rate of ~5 ± 1 mm/yr. A similar average rate was obtained by summation of the offsets of small valleys and other landforms accepted to be Holocene in age by the morphology in the 26-km interval of the southern El-Ghab subsegment between the localities of Sahlie and El-Beida [8]. Thus, this is a relatively stable parameter.

Fivefold GPS measurements carried out in 2004–2008 near the southern and central subsegments of the El-Ghab Fault Zone by the Russian–Syrian RASGORS working group revealed a shear rate of 1 mm/yr in combination with transverse shortening of the southern subsegment and the same shortening without shearing in the central subsegment [4, 44]. Similar GPS measurements performed near El-Ghab for other reference points by an American–Syrian working group in 2000, 2007, and 2008 estimated accumulation of the elastic deformation, which corresponds to a shear rate no higher than 2–3 mm/yr [10]. Thus, two independent studies showed that the rate of contemporary shear in the El-Ghab Fault Zone is less than the average long-term shear rate by a factor of 2–3. However, the aforementioned 12-m offset of the Roman aqueduct constructed across the El-Ghab Zone in the 1st century B.C. or 1st century A.D., no earlier than 63 year B.C., gives an average shear rate of ~6 mm/yr over two millennia. If the contemporary low rate of accumulation of deformation revealed by GPS measurements is inherent not only to the last decade but also for a longer time interval, e.g., the past several centuries, this rate was much higher in the preceding centuries after construction of the aqueduct. Thus, the suggestion that the seismic energy released by earthquakes in the El-Ghab Fault Zone varied in proportion to the gain of elastic deformation is quite plausible.

The distribution of seismic energy released by strong earthquakes during the last two millennia in the south and center of the El-Ghab Fault Zone was compared with similar distributions in the northern subsegment of this zone and with the adjacent part of the EAFZ to the southwest of 39° N and 40° E (Table 2; Fig. 2c). Manifestations of cyclicity with a period of ~300 Ma have been caught in the southwest of the EAFZ like in the south and center of the El-Ghab Fault Zone, but the are expressed less distinctly. This vagueness may be caused by heterogeneity of the EAFZ, which consists of a number of subsegments and subdivides into several branches in the southwest. At the same time, variations with longer periods expressed in amounts of seismic energy released at peak phases of cycles are outlined, but they obey another tendency than in the south and center of the El-Ghab Fault Zone. These quantities reached a maximum in the 3rd–7th centuries with peaks in the 3rd and 6th centuries A.D. close to the time-dependent distribution of seismicity in adjacent parts of the Alpine–Himalayan Belt, where it is known as the Byzantine paroxysm [6]. A gradual decline took place with a minimum in the 14th century and a new increase in released energy with a maximum in the 19th century A.D. Thus, a hypercycle is outlined here, but its period (1300–1600 Ma) and age of similar phases differ from those in the south and center of the El-Ghab Fault Zone. This probably reflects different

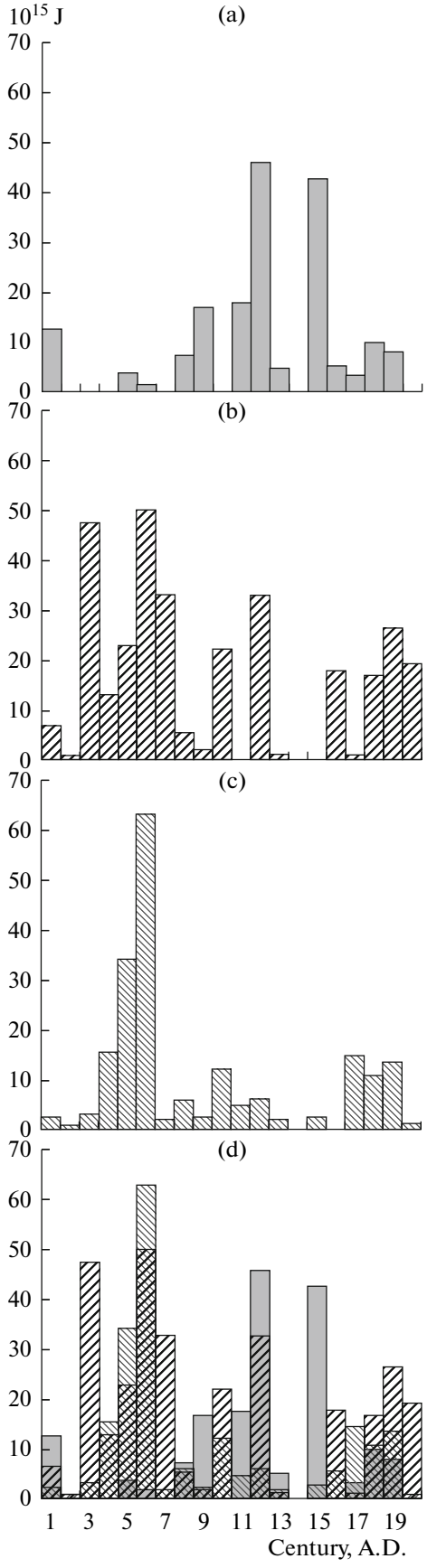

Fig. 2. Bar charts of time-dependent distribution of 100-yr seismic energy released by earthquakes with magnitudes of $M_S \geq 5.7$: (a) southern and central subsegments of El-Ghab Fault Zone; (b) northern segment of same fault zone; (c) Southwestern East Anatolian Fault Zone, (d) combination of bar charts (a)–(c).

variation in stress-and-strain state of the two largest zones in the Near East.

As concerns the northern subsegment of the El-Ghab Fault Zone, the seismic cycles are poorly traced there and long-period variations do not reveal distinct tendencies (Fig. 2b), probably as a result of interference of geodynamic features of the El-Ghab Fault Zone and EAFZ (Fig. 2d).

CENTRAL PART OF THE ALPINE–HIMALAYAN BELT

The summary catalog of strong ($M_S \geq 5.7$) earthquakes presented in [6] and corrected with allowance for new evidence was used to analyze the time-dependent distribution of seismicity in the central part of the Alpine–Himalayan Belt. This catalog comprises the last 5000 years, i.e., the entire late Holocene, and has been compiled based on other catalogs of instrumental and historical earthquakes that occurred in this region, numerous publications on separate seismic events, and information on archeo- and paleoseismicity. The catalog reveals seismic cycles with periods of 300 to 700–800 years in well-studied fault zones, which do not coincide in time. In addition, the catalog, which is completely represented as a bar chart displaying the total release of seismic energy during 50-year time intervals, had made it possible to outline more prolonged variations of seismicity. They, however, have not been reliably substantiated, because of incomplete recording of historical strong earthquakes. The initial data largely concern seismic energy released in the 19th and 20th centuries. In the 20th century, they were recorded instrumentally and included events of great and intermediate depths (>70 km), which were caught unreliably or not recorded at all from historical sources. The completeness of historical evidence decreased back to the recording of single events in the second half of the 1st millennium B.C. Older earthquakes are known only from archeo- and paleoseismological data on a limited number of localities in corresponding investigations were carried out.

To compensate the incompleteness of the seismological record, we introduced two corrections to the interpretation of the catalog [7]. First, taking into account the approximate estimate of unrecorded preinstrumental seismic events argued by Golinsky [2], we increased by one and a half times the amount of seismic energy released in the 18th and 19th centuries as compared with instrumental earthquakes of the 20th century and by two times for earlier seismic events. Second, historical earthquakes have been nor-

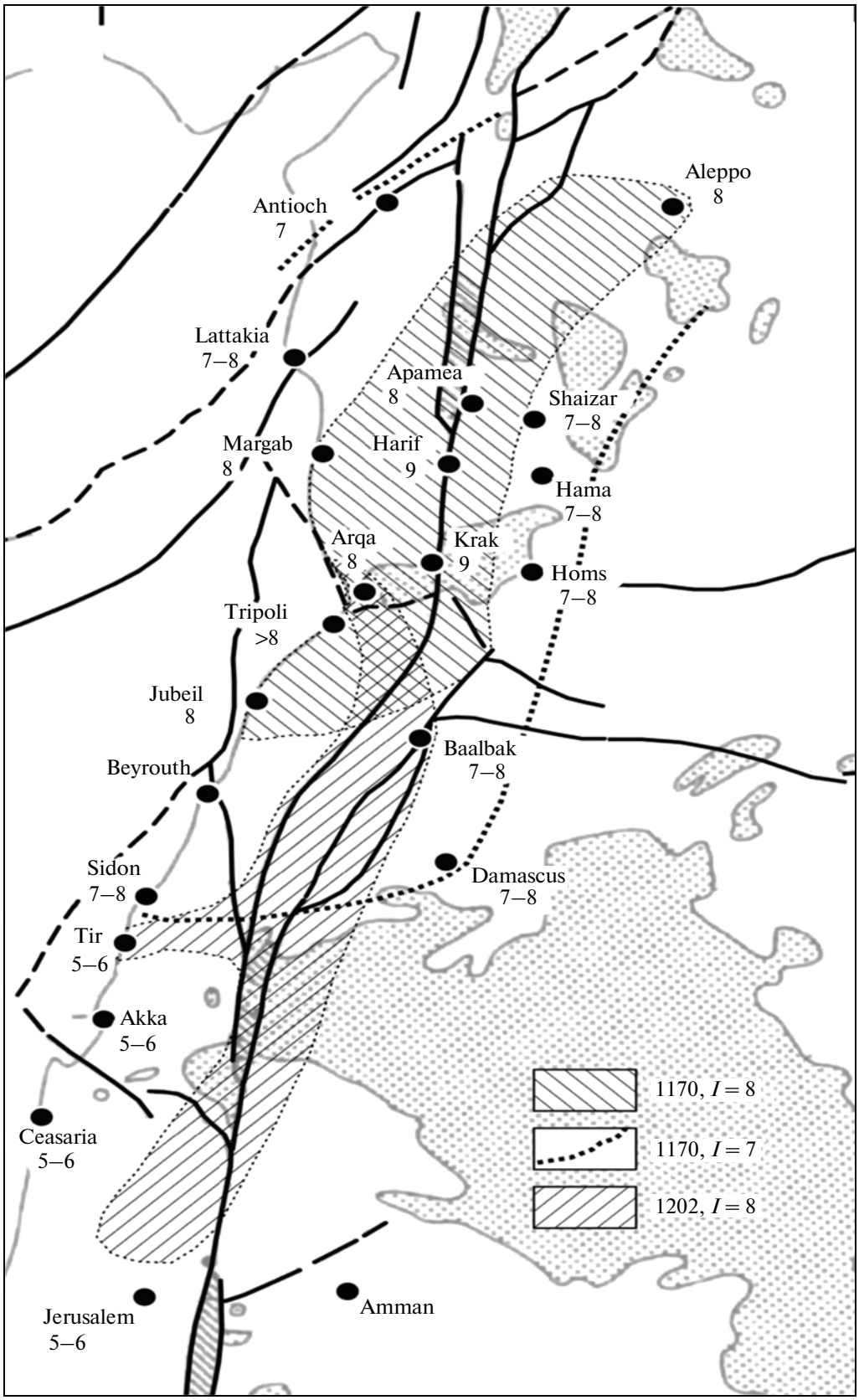

Fig. 3. Map of isoseists for earthquakes of June 29, 1170 [4] and May 20, 1202 [15].

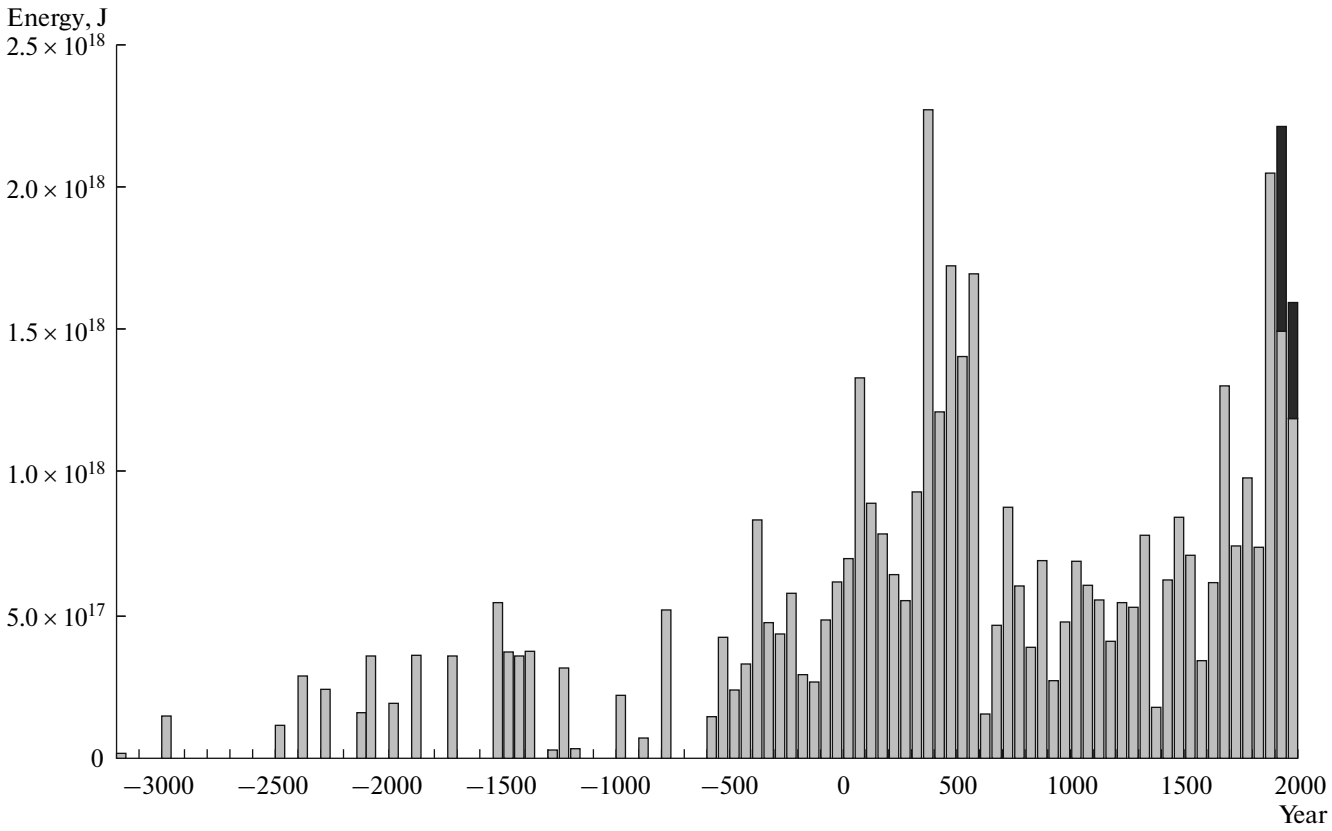

Fig. 4. Bar chart of seismic energy quantity (J) released by earthquakes with $M_S \geq 5.7$ in central part of Alpine–Himalayan Orogenic Belt from 3200 B.C. to end of 20th century A.D. recompiled using correction for incomplete revealing of strong pre-instrumental earthquakes and areas of their stable recording [7]. Bar chart is compiled according to 50-year time intervals. Energy released by intermediate earthquakes (sources are more than 70 km deep) is shown in black.

malized taking into account areas of their stable recording [6, 7].

With introduction of corrections, long-term variations in seismicity were denoted more distinctly (Fig. 4). In addition to a bimodal surge in seismicity from the mid-17th to the mid-20th centuries (a peak in the second half of the 19th century and first half of the 20th century), a surge from the mid-4th to the end of the 6th centuries has been denoted. Archeo- and paleoseismological data presumably outlined a surge in the 15th–13th centuries B.C. These data build up the surge, obliterating the strongest earthquake(s) related to the Great Minoan volcanic eruption on Santorini Island in the second half of the 16th century B.C., which was apparently unlikely in geodynamic nature as compared with other analyzed events. The time intervals between comparable phases were 1250–1300 Ma between surges of the 17th–20th centuries B.C. and within the 1st millennium B.C. and 1800–1850 Ma between the second of them. The two latter chronological intervals are close in the age of the surge to phases of enhanced seismicity in the southwestern EAFZ (Fig. 2). This similarity is understandable, because all regions of stable earthquake recording in the summary catalog occurred before the second millennium A.D. in the eastern Mediterranean and Arabian–Caucasus segments of the Alpine–Himalayan Belt; the EAFZ is a part of this belt.

CONCLUSIONS

As has been established by earlier studies, offsets along fault zones in the domains of high seismic activity are largely made up of displacements during earthquakes, so that slow movements between the earthquakes mostly can be neglected. It was shown that seismicity periodically varies in many active zones, forming seismic cycles hundreds of years in duration. Such cyclicity is explained by periodic overcoming of the ultimate strength of rocks by elastic deformation accumulated in fault zone. This is expressed as a peak in seismicity and does not result in variation in the rate of elastic deformation accumulation, i.e., a change in the stress–strain state of the region. When added together, offsets related to separate earthquakes yield an average rate of displacements along the fault that remains more or less constant.

Our results show that particular active zones and the Arabian–Caucasus segment of the Alpine–Himalayan Orogenic Belt as a whole are characterized by

variations in seismicity longer than the seismic cycles established in the same regions. These variations, which most likely are also cyclical with periods of 1200–1800 years, are called hypercycles. The data on the northern part of the DST (southern and central subsegments of the El-Ghab segment) give grounds to suggest that hypercycles reflect variations in the stress–strain state of the active zone. These periodic variations may be caused by variations in the rate of stored elastic deformation or by variation in the strength of rocks, for example, related to variable permeability and the action of fluids. The causes of hypercyclicity can be discussed only hypothetically. Variations in magnetic field with periods of 1200 and 1800 yr, which eventually can be related to movements at the mantle–core boundary [1], are noteworthy.

In the described cases, hypercyclicity apparently has a wavelike character and because of this does not change the averaged velocities of movements over longer time intervals. However, other situations are also known. For example, a sharp intensification in movements along faults and seismicity has been noted in Fennoscandia in the early Holocene with a peak at 9 ka ago [32]. The intensification is related to superposition of glacioisostatic uplifting on the constant stress system during the last deglaciation (see references in [5]).

Long-term variations in seismicity, which are probably related to a change in the stress–strain state of mobile belts, have both theoretical and practical applications. First, variations in phases of increasing activity can initiate geodynamic processes, which are impossible for the averaged parameters of the system. These can be fast migration of tectonic nappes for significant distances established in some domains of the Alpine–Himalayan Belt. Second, variations in seismicity should be taken into account by estimating the seismic hazard of territories, which is currently based on summary analysis of seismicity over the entire epoch of recorded earthquakes. It has been deemed impossible that an expected maximum magnitude (M_{MAX}) of the future earthquake would be lower than the maximum of the already recorded magnitude. Taking hypercycles into account by probabilistic estimation of seismic hazard, a situation is assumed when in certain time intervals M_{MAX} in the studied territory becomes lower than the highest recorded maximum, so that estimation of M_{MAX} will deviate from the simple linear relationship determined by the summary plot of recurrence. It is still too early to practically recommend the use of seismic hypercycles. The study of hypercycles is still at the very early stage and requires further development.

ACKNOWLEDGMENTS

This study was supported by the Division of Earth Sciences, Russian Academy of Sciences (program no. 6, project "Evolution of the Lithosphere in the Alpine–Himalayan Continental Orogenic Belt in the Late Cenozoic (Oligocene–Quaternary) and Role of Upper Mantle Flows in Its Transformation") and by the Russian Foundation for Basic Research (project no. 11-05-00628-a).

REFERENCES

1. S. P. Burlatskaya, *Archeomagnetism: Study of Ancient Magnetic Field* (Inst. Phys. Earth, Russian Acad. Sci., Moscow, 1987) [in Russian].
2. G. L. Golinsky, *Cand. Sci. (Phys.-Math.) Dissertation* (Inst. Phys. Earth, Russian Acad. Sci., Moscow, 2000).
3. N. K. Karapetyan, *Seismodynamics and Mechanism of Earthquakes in the Armenian Highland* (Izd-vo AN ArmSSR, Yerevan, 1990) [in Russian].
4. *Neotectonics, Recent Geodynamics, and Seismic Hazard in Syria*, Ed. by V. G. Trifonov (GEOS, Moscow, 2012) [in Russian].
5. V. G. Trifonov, *Neotectonics of Eurasia* (Nauchnyi mir, Moscow, 1999) [in Russian].
6. V. G. Trifonov and A. S. Karakhanyan, *Geodynamics and Civilization History* (Nauka, Moscow, 2004) [in Russian].
7. V. G. Trifonov and A. I. Kozhurin, "Study of active faults: Theoretical and applied implications," Geotectonics **44** (6), 510–528 (2010).
8. V. G. Trifonov, V. M. Trubikhin, Zh. Adzhamyan, Z. Jallad, and Yu. El-Hair, "Levantine Fault Zone in Northwestern Syria," Geotektonika **25** (2), 63–75 (1991).
9. S. A. Fedotov, "Seismic cycle, possibilities of quantitative seismic regionalization and long-term seismic prediction," in *Seismic Regionalization of the USSR* (Nauka, Moscow, 1968), pp. 121–150 [in Russian].
10. A. Alchalbi, M. Daoud, F. Gomez, et al., "Crustal deformation in northwestern Arabia from GPS measurements in Syria: Slow slip rate along the northern Dead Sea Fault," in *Abstracts of International Workshop on Active Tectonic Studies and Earthquake Hazard Assessment in Syria and Neighboring Countries* (Damascus, 2009), pp. 23–24.
11. N. N. Ambraseys, "Temporary seismic quiescence: SE Turkey," Geophys. J. **96**, 311–331 (1989).
12. N. N. Ambraseys and M. Barazangi, "The 1759 earthquake in the Bekaa Valley: Implication for earthquake hazard assessment in the eastern Mediterranean region," J. Geophys. Res. **94**, 4007–4013 (1989).
13. N. N. Ambraseys and C. Finkel, *The Seismicity of Turkey and Adjacent Areas: a Historical Review (1500–1800)* (Muhittin Salih, Istanbul, 1995).
14. N. N. Ambraseys and J. A. Jackson, "Faulting associated with historical and recent earthquakes in the eastern Mediterranean region," Geophys. J. Intern. **133** (2), 390–406 (1998).
15. N. N. Ambraseys and C. P. Melville, "An analysis of the eastern Mediterranean earthquake of 20 May 1202," in *Historical Seismograms and Earthquakes of the World*, Ed. by W. Lee (Academic Press, San Diego, 1988).
16. N. N. Ambraseys and C. P. Melville, "Historical evidence of faulting in eastern Anatolia and northern Syria," Ann. Geophys. **38** (3/4), 337–343 (1995).

17. *Archaeoseismology*, Ed. by S. Stiros and R. E. Jones (I.G.M.E. and the British school at Athens, Fitch Lab. Occasional paper 7, Athens, 1996).
18. M. Barazangi, D. Seber, T. Chaimov, J. Best, R. D. Litak, and T. Sawaf, "Tectonic evolution of the northern Arabian Plate in western Syria," in *Recent Evolution and Seismicity of the Mediterranean Region*, Ed. by. E. Boschi, E. Mantovani, and A. Morelli (Kluwer, Dordrecht, 1993), pp. 117–140.
19. A. Ben-Menahem, "Four thousand years of seismicity along the Dead Sea Rift," J. Geophys. Res. **96** (B2), 20195–20216 (1991).
20. M. Berberian, *Natural Hazards and the First Earthquake Catalogue of Iran, Vol. 1: Historical Hazards in Iran Prior to 1900* (UNESCO, Intern. Inst. Earthquake Engineers and Seismology, Tehran, 1994).
21. *Catalogs of Earthquakes by the Harvard Univ.* http://www.seismology.Harvard.edu/
22. "Historical and Prehistorical Earthquakes in the Caucasus," in *Catalogs of Earthquakes*, Compiled by A.S. Karakhanian (Kluwer, Dordrecht, 1997).
23. J. Chorowicz, D. Dhont, O. Ammar, M. Rukieh, and A. Bilal, "Tectonics of the Pliocene Homs basalts (Syria) and implications for the Dead Sea Fault Zone activity," J. Geol. Soc. London **161**, 1–13 (2004).
24. F. Gomez, M. Khawlie, C. Tabet, A. N. Darkal, K. Khair, and M. Barazangi, "Late Cenozoic uplift along the northern Dead Sea Transform in Lebanon and Syria," Earth Planet. Sci. Lett. **241**, 913–931 (2006).
25. *GSHAP Catalog. India and Adjoining Areas. National Geophysical Data Center.* www.ngdc.noaa.gov
26. E. Guidoboni, A. Comastri, and G. Traina, *Catalogue of Ancient Earthquakes in the Mediterranean Area up to the 10th Century* (Istituto Naazionale di Geofisica, Rome, 1994).
27. A. S. Karakhanian, V. G. Trifonov, T. P. Ivanova, A. Avagyan, M. Rukieh, H. Minini, A. E. Dodonov, and D. M. Bachmanov, "Seismic deformation in the St. Simeon Monasteries (Qal'at Sim'An), Northwestern Syria," Tectonophysics **453**, 122–147 (2008).
28. V. Karnik, *Seismicity of the European Area, Pt. I, II* (Acad. Publ. House of the Czechosl. Acad. Sci., Prague, 1968).
29. *New Catalog of Strong Earthquakes in the USSR from Ancient Times through 1977*, Ed. by N. V. Kondorskaya and N. V. Shebalin (World Data Center A for Solid Earth Geophysics, NOAA, Boulder, 1982).
30. *Special Catalogue of Earthquakes of the Northern Eurasia (SECNE)*, Ed. by N. V. Kondorskaya and V. I. Ulomov (Global Seismic Hazard Asssessment Program, Zurich, 1995). http://www.seismo.ethz.ch/gshap/neurasia/nordasiacat.txt
31. M. Meghraoui, F. Gomez, R. Sbeinati, J. Van der Woerd, M. Mouty, A. N. Darkal, Y. Radwan, I. Layyous, H. Al-Najjar, R. Darawcheh, F. Hijazi, R. Al-Ghazzi, and M. Barazangi, "Evidence for 830 years of seismic quiescence from palaeoseismology, archaeoseismology and historical seismicity along the Dead Sea fault in Syria," Earth Planet. Sci. Lett. **210**, 35–52 (2003).
32. N.-A. Mörner, *Paleoseismicity of Sweden* (JOFO Grafiska AB, Stockholm, 2003).
33. *Earthquake Data Base (NEIC, NOAA, PRE, PRE-Q, NEIS, Advanced National Seismic System ANSS)*, (National Earthquake Information Center, USGS, Golden, 2010), http://neic.usgs.gov/
34. B. Papazachos and C. Papazachou, *The Earthquakes of Greece* (Editions Ziti, Thessaloniki, 1997).
35. J. Plassard and B. Kogoj, "Seismisité du Liban: catalogue des séismes ressentis," 3rd ed., in *Collection des Annales-Memoires de l'Observatoire de Ksara* (Conseil National Libanais de la Recherche Scientifique, Beyrouth, 1981), Vol. 4: seismologie, cahier 1.
36. J. P. Poirer and M. A. Taher, "Historical seismicity in the Near and Middle East, North Africa, and Spain from Arabic documents (VII–XVIII Centuries)," Bull. Seismol. Soc. Amer. **70** (6), 2185–2201 (1980).
37. M. Rukieh, V. G. Trifonov, A. E. Dodonov, H. Minini, O. Ammar, T. P. Ivanova, T. Zaza, A. Yusef, M. Al-Shara, and Y. Jobaili, "Neotectonic map of Syria and some aspects of Late Cenozoic evolution of the northwestern boundary zone of the Arabian Plate," J. Geodyn. **40**, 235–256 (2005).
38. M. R. Sbeinati, R. Darawcheh, and M. Mouty, "The historical earthquakes of Syria: An analysis of large and moderate earthquakes from 1365 B.C. to 1900 A.D.," Ann. Geophys. **48** (3), 347–435 (2005).
39. M. R. Sbeinati, M. Meghraoui, G. Suleyman, F. Gomez, H. Al-Najjar, and R. Al-Ghazzi, "Timing of earthquake ruptures at the Al-Harif Aqueduct (Dead Sea Fault) from archaeoseismology, paleoseismology and tufa cores," in *Abstracts of Intern. Workshop on Active Tectonic Studies and Earthquake Hazard Assessment in Syria and Neighboring Countries* (Damascus, 2009), p. 78.
40. H. Soysal, U. S. Sipahioglu, D. Kolcak, and Y. Altdiok, *Turklye ve cevbesimi tabihsel depbim katalogu. Tuklye biumsel ve teknik arastirma kurumu matematik-fiziki ve biolojik bilimler arastieka grubu* (TMG, Projeco, 1997) (in Turkish).
41. M. A. Taher, Corpus des textes arabes relatits aux tremblements de terre et autres catastrophes naturelles de la conquéte arabe au XII H./XVIII JC, *Thesis de Doctorat d'Etat* (Sorbonne Univ., Paris, 1979).
42. T. Taymaz, H. Eyidogan, and J. Jacjsib, "Source parameters of large earthquakes in the East Anatolian Fault Zone (Turkey)," Geophys. J. Intern. **106** (3), 537–550 (1991).
43. H. Tiedemann, *Catalogue of Earthquakes and Volcanic Eruptions*, Zurich: Swiss Reinsurance, 1991).
44. V. G. Trifonov, A. E. Dodonov, A. S. Karakhanian, T. P. Ivanova, D. M. Bachmanov, O. Ammar, M. Rukieh, H. Minini, A.-M. Al-Kafri, O. Ali, Sh. Al-Yusef, A. Yusef, T. Zaza, and M. Ali, "Seismotectonics of Syria and surrounding areas," in *Abstracts of Intern. Workshop on Active Tectonic Studies and Earthquake Hazard Assessment in Syria and Neighboring Countries* (Damascus, 2009), pp. 66–67.
45. Ch. D. Walley, "A braided strike-slip model for the northern continuation of the Dead Sea fault and its implications for Levantine tectonics," Tectonophysics **145**, 63–72 (1988).

Reviewers: A.E. Rogozhin and A.M. Korjenkov

Translated by V. Popov